

DOI: 10.1070/QEL16039

Propagation effects in highly ionised gas media

V. Tosa, K. Kovács, B. Major, E. Balogh, K. Varjú

Abstract. **The problem of propagation of an ultraintense pulse in a gas medium is solved by using a 3D nonadiabatic model extended to the case of multiple ionisation of atoms in the interaction region. A complex space–time coupling of the pulse during its propagation and strong spatial and temporal changes in the field distribution are shown.**

Keywords: *intense laser pulse, ionisation of a gas medium, propagation problem.*

1. Introduction

Propagation of intense laser pulses in ionising media is important in a wide range of applications, including laser-driven accelerators [1], laser-plasma channelling [2], high order harmonic generation [3], supercontinuum generation [4], X-ray lasers and laser-fusion schemes (see review [1]).

An intense laser pulse propagating in a neutral gas is affected by diffraction, refraction and nonlinear effects like self-focusing or self-phase modulation (SPM), ionisation and plasma defocusing [5–7]. As the beam focuses, the increased intensity results in ionisation of a medium and plasma formation; hence, both linear and nonlinear effects of propagation will be altered. Propagation of a light bullet in an ionising medium proves to be a highly nonuniform process both in time and in space. In time the leading edge of the pulse will propagate in a neutral gas, being affected only by diffraction and neutral dispersion. As intensity increases in the pulse, the following part will be suffering from nonlinear effects (like SPM) governed by the nonlinear refractive index (n_2) of neutrals. Furthermore, for high-power laser pulses ionisation starts already on the leading edge of the pulse, and following parts of the pulse will propagate through an ionised medium, the ionisation rate depending strongly on time, and so both linear and nonlinear parameters of the medium will become time-dependent. The trailing edge of the pulse will be influenced by effects of the ionised medium, accompanied by defocusing in certain cases and by refocusing in others. The degree of the above modifications will vary in the radial direction, which will produce complex time–space coupling during pulse propagation.

When an ultrashort, intense laser pulse is used in particle acceleration experiments, spatial and energy distributions of energetic electrons are shown [8, 9] to depend strongly on the contrast ratio and shape of the laser prepulse. However, this implies that it is essential to estimate the modifications of the shape of the pulse as induced during propagation. Moreover, the distortions induced in the temporal and spatial pedestal of an ultraintense pulse are important in these experiments and should be quantified both for characterising the pulse and for estimating the electron concentration map to be used further in PIC simulations [9].

An active field where the propagation of an intense pulse plays an essential role is generation of high order harmonics and attosecond pulses, either single or in trains. High harmonic generation (HHG) is a very perspective method for transforming the properties of IR laser pulses to the XUV or soft-X-ray regime, thus providing unique ultrashort coherent pulses with high photon energies. Unfortunately, the conversion efficiency on a single atom level is rather weak, and so harmonic radiation from many atoms has to be added constructively in order to achieve a flux level necessary in pump-probe experiments.

The rapidly increasing laser pulse powers give promise to the HHG in increasing magnitude, if macroscopic conditions can be chosen suitably. One option for scaling up the HHG is a geometrical enlargement [10, 11], keeping the system in the low ionisation regime. With the peak powers promised to become available in the new laser facilities (ELI, CALA, EXCELS) this method will soon become unpractical due to the required focusing of tens-to-hundred metres. An alternative method for utilising these high power laser pulses is highly ionised arrangements, where phase matching is achieved in a high density, short gas target. The two alternatives require different focusing arrangements and different gas targets, and direct experimental comparison is not available in any of the existing laboratories, let alone in the new infrastructures under development. Thus a theoretical/simulation experiment is the only means to compare the properties of the high harmonic radiation produced under low and high ionisation conditions.

Recently, efficient soft X-ray HHG in multiply ionised plasmas [12] has been reported. Using intense UV driving

V. Tosa, K. Kovács National Institute for R&D of Isotopic and Molecular Technologies, Cluj-Napoca, Romania; ELI-ALPS, ELI-HU Nkft, Szeged, Hungary; e-mail: tosa@itim-cj.ro;
B. Major Department of Optics and Quantum Electronics, University of Szeged, Szeged, Hungary;
E. Balogh Department of Optics and Quantum Electronics, University of Szeged, Szeged, Hungary; Center for Relativistic Laser Science, Institute for Basic Science (IBS), Gwangju, Republic of Korea;
K. Varjú ELI-ALPS, ELI-HU Nkft, Szeged, Hungary; Department of Optics and Quantum Electronics, University of Szeged, Szeged, Hungary

Received 24 February 2016
Kvantovaya Elektronika **46** (4) 321–326 (2016)
Submitted in English

lasers at 270 nm, emission in the soft X-ray domain was obtained and assumed to be generated by ions, from Ar^+ to Ar^{5+} ions. The authors of [12] emphasise the necessity to model pulse propagation in these media of multiple ionised atoms as well as to model harmonic generation in these conditions.

In this paper we use a three dimensional nonadiabatic model to characterise ultrashort pulse propagation in a gas medium under conditions of high intensities, which creates high electron concentrations via multiple ionisations of the target atom. Although nonsequential multiple ionisation has been reported to occur in noble gases [13], the dominant mechanism is sequential ionisation; therefore, to calculate the electron concentration we adopt a scheme that relies on rates of successive single-electron ionisation events [14]. Models for pulse propagation in gas or condensed media are reviewed in [15] including numerical modelling of ultrashort pulse propagation in extreme nonlinear regimes.

2. Model

Propagation of an ultrashort pulse in an ionising gas medium can be described in cylindrical coordinates by the equation [16]:

$$\nabla^2 E_1(r,z,t) - \frac{1}{c^2}\frac{\partial^2 E_1(r,z,t)}{\partial t^2} = \frac{\omega^2}{c^2}(1-\eta_{\text{eff}}^2)E_1(r,z,t), \quad (1)$$

where c is the speed of light; E_1 is the full electric field (carrier) with centre frequency ω;

$$\eta_{\text{eff}}(n_a,n_e,r,z,t) = \eta_0(n_a) + \eta_2(n_0)E_1^2(r,z,t) - \frac{\omega_p^2(n_e,r,z,t)}{2\omega^2} \quad (2)$$

is the effective refractive index, which accounts for the dispersion by neutrals and electron plasma [first and respectively last term of Eqn (2)] as well as for the nonlinear refractive index associated with the bound electrons [second term in Eqn (2)]; and ω_p is the plasma frequency, which is proportional to the electron concentration n_e.

To solve Eqn (1) it is advantageous to write it in a moving coordinate frame ($z' = z$ and $t' = t - z/c$). Hereafter, we drop the prime symbol for simplicity, so that the equation takes the form:

$$\nabla^2 E_1(r,z,t) - \frac{1}{c^2}\frac{\partial^2 E_1(r,z,t)}{\partial z \partial t} = \frac{\omega^2}{c^2}(1-\eta_{\text{eff}}^2)E_1(r,z,t). \quad (3)$$

The time derivative can be eliminated by applying the Fourier transform. Also expanding the Laplace operator, the equation is expressed as:

$$\left(\frac{\partial^2}{\partial r^2} + \frac{1}{r}\frac{\partial}{\partial r} + \frac{\partial^2}{\partial z^2}\right)E_1(r,z,\omega) - \frac{2i\omega}{c^2}\frac{\partial E_1(r,z,\omega)}{\partial z} = \frac{\omega_2}{c^2}\hat{F}\left[(1-\eta_{\text{eff}}^2)E_1(r,z,t)\right], \quad (4)$$

where $\hat{F}$ is the Fourier transform operator. In the paraxial approximation the second derivative in z is neglected; therefore, the final equation to be solved numerically is:

$$\left(\frac{\partial^2}{\partial r^2} + \frac{1}{r}\frac{\partial}{\partial r}\right)E_1(r,z,\omega) - \frac{2i\omega}{c^2}\frac{\partial E_1(r,z,\omega)}{\partial z} = \frac{\omega^2}{c^2}\hat{F}\left[(1-\eta_{\text{eff}}^2)E_1(r,z,t)\right]. \quad (5)$$

To solve Eqn (5) numerically we use a Crank–Nicolson method written for a nonlinear scale in the radial direction. The Crank–Nicolson method ensures sufficient accuracy in dealing with finite differences while the nonlinear scale allows a sufficiently large integration domain in order to avoid unphysical reflections of the propagated field on the domain walls. The right-hand side in Eqn (5) has both an explicit dependence of the solution and an implicit one through the plasma term and Kerr term. For this reason, we followed an iterative self-consistent procedure at each step of integration. After integrating over a dz step we obtain the propagated field E_1 in the frequency domain. Then, we use the inverse Fourier transform to obtain E_1 in the time domain and recalculate the free term in Eqn (5). After it we repeat the integration in the frequency domain with the new source term and proceed like this until the difference between two successive laser fields is below a given threshold. Usually three to five iterations are enough, but this depends on many parameters such as the number of steps in the z direction, the initial gas pressure, initial intensity, etc.

The imaginary part of the refractive index was also considered in order to estimate the damping of the wave during propagation. We assume that the energy lost by the pulse is caused solely by the supply energy spent on ionisation. To find this contribution we extended the method described in [17] for single ionisation to the multiple ionisation case. In short we write the energy balance for the ionisation process and assume that the energy lost by the pulse between z and z + dz is the opposite of the energy gained by the electrons in the same interval. The energy loss was estimated for each (r, z) point after every successful integration step, and the dumped field was used in the next integration step.

To integrate Eqn (5) in realistic conditions an essential ingredient is the ionisation model used to calculate the ionisation rates. One possible way to proceed for molecules and atoms, also adopted for the present results, is to use the Ammosov–Delone–Krainov (ADK) [18] model or its molecular version [19].

As one can see from Eqn (2) we need to estimate the electron concentration in the medium, which, in a low intensity field (10^{14} W cm^{-2}), originates from single (usually multiphoton or tunnel) ionisation of atoms/molecules. In a very intense laser field an atom/molecule experiences multiple stripping of electrons, starting from the outer shell ones. To calculate the electron concentration we considered only sequential ionisations and developed a system of rate equations which allows the calculation of fractions of ionic species assuming the following known quantities: n_0 is the initial density of the medium; $w_{01}(t)$, $w_{12}(t)$, … are the ionisation rates; index pairs $(k-1)k$ denote the ionisation rate from the $(k-1)$-times ionised species to k-times ionised ones; and the rates were calculated using the ADK [19] approximation. The unknowns are

$n_0(t)$, $n_1(t)$, ..., $nk(t)$, i.e., the fractions of neutrals, singly ionised, …, k-times ionised species.

The following system of differential equation was written and solved:

$$\frac{dn_0(t)}{dt} = -n_0(t)w_{01}(t),$$

$$\frac{dn_1(t)}{dt} = n_0(t)w_{01}(t) - n_1(t)w_{12}(t),$$

$$\vdots$$

$$\frac{dn_z(t)}{dt} = n_{z-1}(t)w_{(z-1)z}(t).$$

In order to correctly evaluate the variation of the effective refractive index due to the plasma contribution, we calculate the total number of electrons resulting from this consecutive stripping of an atom/molecule:

$$n_e(t) = \sum_{k=1}^{z} kn_k(t).$$

One brief mention should be made for the optical Kerr term in Eqn (2). As multiple ionised species are present in a gas, one should account for their contribution to the third order susceptibility χ_3 of the medium. The values of the susceptibilities for ionised atoms are not known but can be estimated. Here we used the relationship that can be established [20] between the susceptibility of the ion χ_3^+ and the susceptibility of the neutral atom χ_3^0, their ratio being in connection with the ratio of their ionisation potentials as $\chi_3^+/\chi_3^0 \approx (I_p^0/I_p^+)^3$, where I_p are the ionisation potentials of the species involved.

3. Results and discussion

In the following we will focus our discussion on the case of an 800-nm femtosecond pulse propagating in Ne at 85 Torr along a 5 mm long static cell placed in the focus. Other parameters of the calculation are as follows: pulse energy 40 mJ, pulse duration 26 fs, focal length 4 m, and beam waist at the focusing element 15 mm. With these conditions the waist in the focus is 68 μm and the initial intensity at medium entrance reaches the value of 1.8×10^{16} W cm^{-2}. At the entrance in the cell the pulse arrives in a Gaussian shape.

Figure 1 plots the time evolution of ionising species Ne, Ne^+, Ne^{2+}, and Ne^{3+} that are fully depleted by the end of the pulse, while Ne^{3+} and Ne^{4+} share the initial population between them. It is clear that for higher intensities one will have to consider higher and higher ionised species. If the initial density n_e is assumed to be equal to n_0, then the final electron concentration will exceed $3n_0$. This is seen in Fig. 2 where the electron concentration and laser envelope are plotted against time. As one can note the electron concentration exhibit three plateaus, the first one around $-6T_0$ (corresponding to double ionisation), the second around $-4T_0$ (corresponding to triple ionisation) and the third one after a peak maximum, related to the time evolution of the ionising species (Fig. 1). This temporal variation of the electron concentration is highly nonuniform in space and thus one can foresee a complex spatiotemporal variation of the refractive index which will cause interesting effects during propagation as we will see in the following.

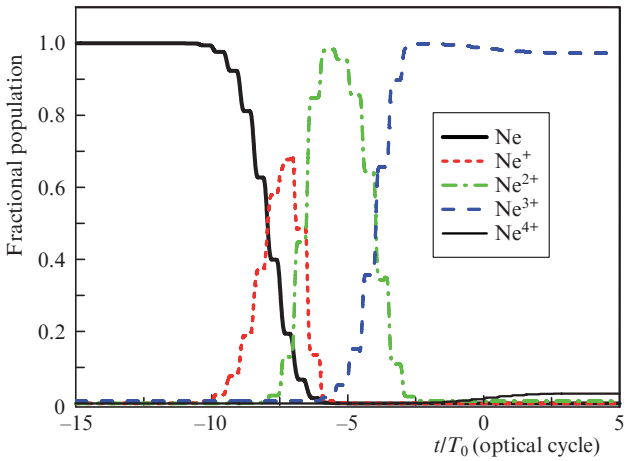

Figure 1. Temporal evolution of the relative concentration of ionised species starting from neutral Ne, for a peak intensity of 1.8×10^{16} W cm^{-2}.

The Gaussian incident pulse becomes temporally distorted during propagation in the ionised Ne medium, and we can evaluate this in all the grid points of the interaction region. Plotted in Fig. 3 is the spatial map of the peak intensity of the laser pulse, from which two main features are worth to be emphasised: the first one is the strong defocusing of the field during propagation, as electron distribution along the radial direction acts as a diverging lens across the beam. The second one is the pulse refocusing on the axis, after ~1.5 mm of propagation. Analysis of the field in detail shows that this is due to the refractive index variation in time. In the leading part of the pulse the variation is given mainly by the electron density variation; however, when electron density comes to a stationary value the main variation of the refractive index is given by the Kerr term. This acts as a converging lens and induces a focusing of the pulse in the trailing edge, after the pulse centre. One can also observe that in the peripheral regions ($r > 250$ μm) and after $z = 4$ mm of propagation we

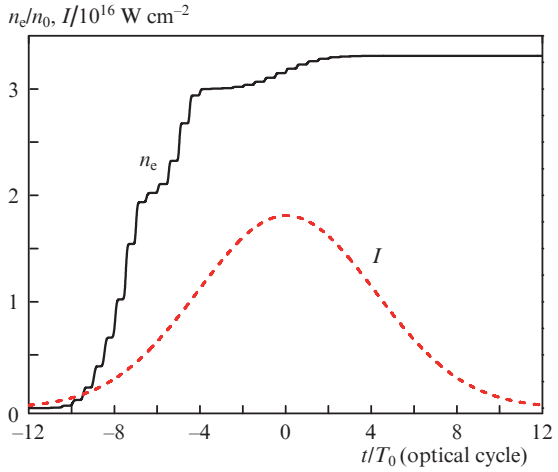

Figure 2. Intensity envelope and electron concentration as a function of time.

could not avoid numerical boundary reflections on the domain walls, but they are weak and do not influence the values of the field in the central part. Probably for longer propagation distances these reflections become important and should be accounted for and eliminated.

It is also interesting to analyse the electron concentration in the integration domain (Fig. 4). One can see the level of ionisation which indicates that even Ne^{3+} is ionised. Also, the plateaus which are seen in time in Fig. 2 are present also here in space, which is another indication that there is a strong space–time coupling during pulse propagation in high ionising conditions.

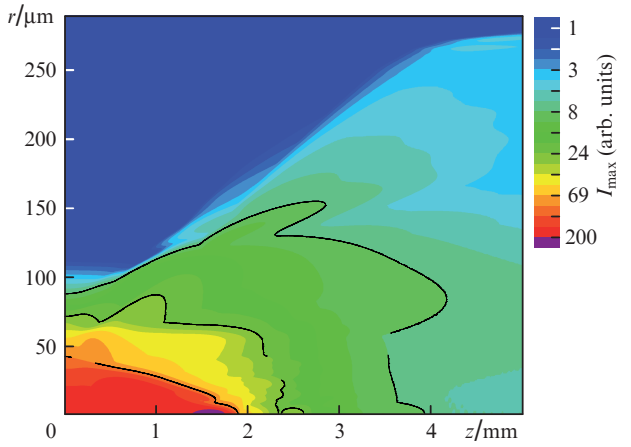

Figure 3. (Colour online) Spatial map of the pulse peak intensity, in units of 10^{14} W cm^{-2}.

The spectral/temporal distortions which the pulse suffers during propagation in the ionising medium will be inherited in all interactions of the laser field with matter. It is therefore essential to characterise these distortions in temporal, spectral and spatial domains, as they could be important even at an optical cycle level. The model we use allows this characterisation because the result of the calculation is the full electric field $E_1(r,z,t)$ or its spectral counterpart $E_1(r,z,\omega)$. We show in Fig. 5 the field in time, on-axis, both at the medium entrance and medium exit. As we see, the pulse experienced heavy changes in both amplitude (due to plasma defocusing) and phase (due to the time variation of the refractive index). An exception is the pulse leading part which did not produce ionisation and is only slightly changed by dispersion of neutrals.

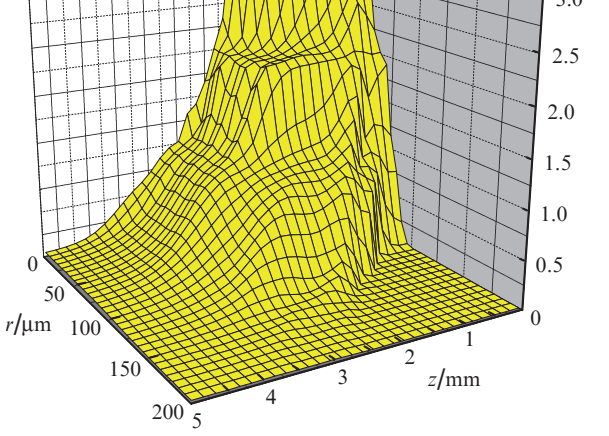

Figure 4. Electron fraction map in units of initial neutral concentration.

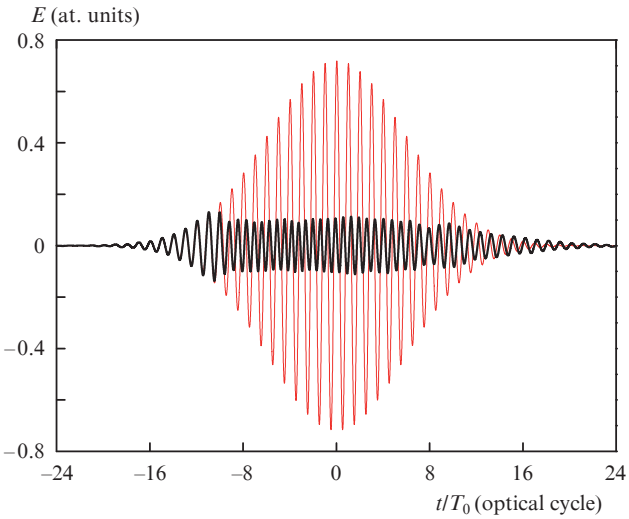

Figure 5. Laser pulse on-axis both at medium entrance (thin curve) and at medium exit (thick curve).

Strong modifications can be seen also in the frequency domain, as shown in Fig. 6. The initial spectrum is a Gaussian centred at 800 nm, while the spectrum at the medium exit on-axis is heavily broadened, both towards longer but especially towards shorter wavelengths. This broadening arises due to plasma induced self-phase modulation, similar to Kerr induced self-phase modulation. The range of broadening is noticeable, from an initial bandwidth of

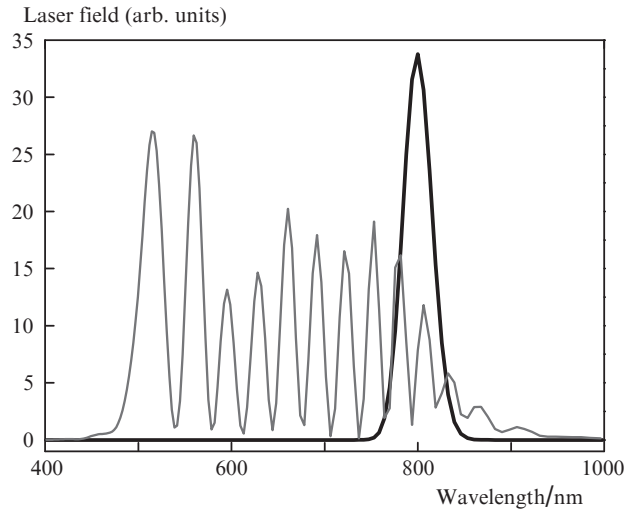

Figure 6. Pulse spectrum at the medium entrance (thin curve) and exit (thick curve).

50 nm centred around 800 nm (transform limited pulse), the pulse extends in a spectral domain from 470 to 950 nm after propagation.

For the generation of high-order harmonics the temporal variations of the optical parameters of the medium give rise to macroscopic phase-matching effects that can, among others, limit the time window of an effective signal [21]. In the high intensity regime present in the first part of the gas medium, high-order harmonics can be generated both from neutrals (at the leading edge of the pulse) and from ions (after neutrals are ionised). However, in our case the high electron density prevents phase-matching of harmonics generated from ions. In fact, in this regime the main contribution to phase-mismatch comes from the plasma refractive index. However, the high-intensity regime can be explored by using UV generating fields, in which case the plasma dispersion is significantly decreased and the linear and nonlinear refractive indices of ions are much larger, and cannot be neglected anymore, as was recently demonstrated in [12].

With near-IR generating fields, phase-matched HHG is mainly restricted to moderate ionisation rates. The strong spatial and temporal distortions of the generating field can create conditions of efficient harmonic generation after a significant propagation length, i.e. after which the nonlinear effects diffracted the laser beam to a wider area in the gas cell, and a homogenous intensity-distribution is achieved. This effect can be nicely seen in Fig. 7 where the map of the peak intensity over the interaction region is plotted. After propagating for about 3 mm the field stabilises to a configuration with a constant intensity and phase over a large region in the radial direction. It is interesting to note that stabilisation starts from peripheral regions towards on-axis.

The space–time coupling can also generate field configurations which give rise to unique effects in the interaction between light and matter. One example is the generation of single attosecond pulses in a lighthouse configuration, which was reported in [22]. In this case it was demonstrated numerically that a multicycle laser pulse (800 nm, 25 fs) gains, in conditions of high ionisations, a rotating wavefront which, generating high order harmonics in interaction with Ar atoms, produce single attosecond pulses in successive half-cycles and with increasing divergence. The overall effect is a series of single attosecond pulses emitted in conical shapes of increasing angles, from one half-cycle to the next half-cycle.

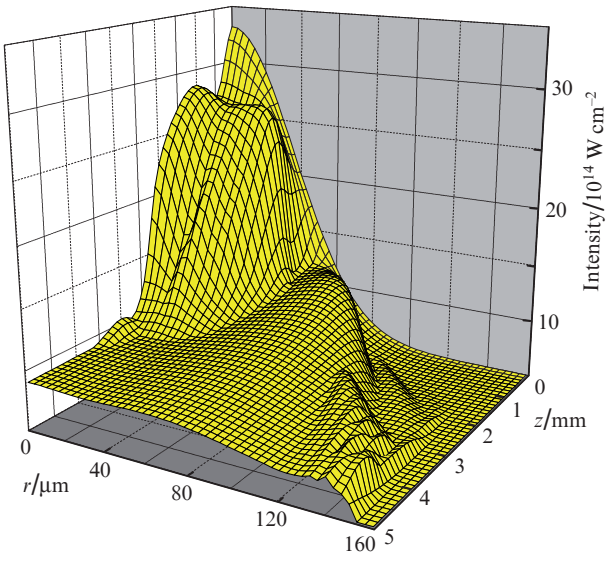

Figure 7. Spatial map of the pulse peak intensity.

4. Conclusions

Thus, the problem of an ultraintense pulse propagating in gaseous media is solved by a 3D nonadiabatic model which was extended to the case of multiple ionisation for the atomic species present in the interaction region. The results demonstrate a complex space–time coupling during pulse propagation and strong temporal/spectral modifications of the pulse. The field configuration can, in specific conditions, generate interesting effects, attosecond lighthouse emission being demonstrated for the case of Ar.

Acknowledgements. V.T. and K.K. gratefully acknowledge financial support from projects RO-CERN E02 (PULSE-PROPAG) and PN-II-ID-PCE-2012-4-0342. The ELI-ALPS project (GOP-1.1.1-12/B-2012-000, GINOP-2.3.6-15-2015-00001) is supported by the European Union and co-financed by the European Regional Development Fund. B.M. and E.B. have been financed by the Hungarian Scientific Research Fund (OTKA NN107235).

References

1. Esarey E., Schroeder C.B., Leemans W.P. *Rev. Mod. Phys*., **81**, 1229 (2009).
2. Min Chen, Ji Luo, Fei-Yu Li, Feng Liu, Zheng-Ming Sheng, Jie Zhang. *Light: Science & Applications*, **5**, e16015 (2016).
3. Krausz F., Ivanov M. *Rev. Mod. Phys*., **81**, 163 (2009).
4. Serebryannikov E.E., Goulielmakis E., Zheltikov A.M. *New J. Phys*., **10**, 093001 (2008).
5. Efimenko E.S., Kim A.V., Quiroga-Teixeiro M. *Phys. Plasmas*, **18**, 032107 (2011).
6. Rae S.C., Burnett K. *Phys. Rev. A*, **46**, 1084 (1992).
7. Rae S.C. *Opt. Commun.*, **104**, 330 (1993).
8. Hosokai T., Kinoshita K., Zhidkov A., Nakamura K., Watanabe T., Ueda T., Kotaki H., Kando M., Nakajima K., Uesaka M. *Phys. Rev. E*, **67**, 036407 (2003).
9. Kim H.T., Pae K.H., Cha H.J., Kim I.J., Yu T.J., Sung J.H., Lee S.K., Jeong T.M., Lee J. *Phys. Rev. Lett*., **111**, 165002 (2013).
10. Rudawski P., Heyl C.M., Brizuela F., Schwenke J., Persson A., Mansten E., Rakowski R., Rading L., Campi F., Kim B., Johnsson P., Huillier A.L., Rudawski P., Heyl C.M., Brizuela F., Schwenke J., Persson A., Mansten E. *Rev. Sci. Instrum*., **84**, 073103 (2013).
11. Heyl C.M., Coudert-Alteirac H., Miranda M., Louisy M., Kovacs K., Tosa V., Balogh E., Varjú K., L'Huillier A., Couairon A., Arnold C.L. *Optica*, **3**, 75 (2016).
12. Popmintchev D., Dollar F., Mancuso C., Chen M., Hankla A., Gao X., Shim B., Gaeta A.L., Tarazkar M., Romanov D.A., Levis R.J., Gaffney J.A., Foord M., Libby S.B., Jaron-Becker A., Becker A., Plaja L., Murnane M.M., Kapteyn H.C., Popmintchev T. *Science*, **350**, 1225 (2015).
13. Larochelle S., Talebpour A., Chin S.L. *J. Phys. B, At. Mol. Opt. Phys.,* **31**, 1201 (1999).
14. Martínez P.G.A., Bergé L. *J. Phys. B, At. Mol. Opt. Phys.*, **47**, 204017 (12pp) (2014); Martínez P.G.A., La Fontaine A.C., Köhler C., Bergé L. *J. Phys. B, At. Mol. Opt. Phys*., **48**, 094010 (2015).

15. Kolesik M., Moloney J.V. *Rep. Prog. Phys.*, **77**, 016401 (2014); Couairon A., Brambilla E., Corti T., Majus D., Kolesik M. *Eur. Phys. J. Spec. Top.*, **199**, 5 (2011).
16. Tosa V., Kim K.T., Nam C.H. *Phys. Rev. A*, **79**, 043828 (2009).
17. Takahashi E., Tosa V., Nabekawa Y., Midorikawa K. *Phys. Rev. A*, **68**, 023808 (2003).
18. Ammosov M.V., Delone N.B., Krainov V.P. *Zh. Eksp. Teor. Fiz.*, **91**, 2008 (1986) [*Sov. Phys. JETP*, **64**, 1191 (1986)].
19. Tong X.M., Zhao Z.X., Lin C.D. *Phys. Rev. A*, **66**, 033402 (2002).
20. Sprangle P., Esarey E., Hafizi B. *Phys. Rev. Lett.*, **79**, 1049 (1997).
21. Schutte B., Weber P., Kovacs K., Balogh E., Major B., Tosa V., Han S., Vrakking M.J.J., Varju K., Rouzee A. *Opt. Express*, **23**, 33947 (2015).
22. Tosa V., Lee J.S., Kim H.T., Nam C.H. *Phys. Rev. A*, **91**, 051801(R) (2015).